e-ISSN 2757-5195

*Çanakkale Onsekiz Mart University*
*Journal of Advanced Research in Natural and Applied Sciences*
*Open Access*

doi.org/10.28979/jarnas.841993 2021, Cilt 7, Sayı 2, Sayfa: 172-181 dergipark.org.tr/tr/pub/jarnas

# Comprehensive Analysis of Alpha-Parametric Set for the Calculation of Intersection Lengths of Radiological Ray Path in Siddon's Algorithm Used in 3D Image Reconstruction

Adem Polat[1*]

[1]Department of Electronics Engineering, Çanakkale Onsekiz Mart University, Çanakkale, Turkey

**Article History**
*Received:* 16.12.2020
*Accepted:* 04.05.2021
*Published:* 30.06.2021
***Research Article***

**Abstract –** The Siddon algorithm is one of the radiological ray path (x-ray) calculation tools used in 3D image reconstruction in medical imaging. In the algorithm, a set of alpha-parametric values is computed containing the length and index values where the voxel array of the x-ray intersects the x-y-z axes. In the alpha-set creation section of the Siddon algorithm, the set elements are sorted from small to large, but some elements have been noticed to have the same value in simulations. These elements are used to calculate which voxels are hit by the ray along the radiological path and at what ratio, but it was recognized that some values of the set were zero, which means some rays did not intersect some voxels at all. This situation may lead to data loss in 3D image reconstructions in medical imaging such as digital breast tomosynthesis (DBT) and computed tomography (CT) especially for huge dimensions such as size up to 800×800×50. Considering the mentioned problems, in this study, the effect of using or eliminating the same repetitive values in the alpha parametric set of the Siddon algorithm on calculations was investigated. To prove our proposal, we performed 3D image reconstruction (lossless and lossy) of a synthetic phantom at a size of 100×100×50. Using special functions that do not take into account the duplicate values in the algorithm, excluding the duplicate values from the calculation solved the stated problems (lossless reconstruction). In this way, data loss that may occur in 3D image reconstruction was reduced since voxel indices and intersection lengths were matched correctly and meaningfully.

***Keywords*** *– Computed tomography, digital breast tomosynthesis, siddon algorithm, x-ray, 3D image reconstruction*

## 1. Introduction

Mainly, iterative and analytical image reconstruction methods are applied in medical imaging modalities such as the optoacoustic tomography (OAT) (or photoacoustic tomography (PAT)) (Paltauf et al., 2002; Wang et al., 2012), the optical tomography (OT) (Dekker, Battista, & Jordan, 2017; Klose & Hielscher, 1999), the diffuse optical tomography (DOT) (Üncü et al., 2017; Sevim et al., 2017; Mercan et al., 2017; Mercan et al., 2019), the computed tomography (CT) (Sidky et al., 2006; Biguri et al., 2017) and the digital breast tomosynthesis (DBT) (Oliveira et al., 2016; Polat & Yildirim, 2018; Polat et al., 2019a). The CT, developed by Hounsfield and Cormack in the 1970s (Nobel Media AB, 2014; Raju, 1999), enables three-dimensional (3D) images of the examined part of the body like the head, chest, and breast. The DBT, an advanced form of x-ray mammography evolved by Gershon-Cohen and others (Kopans, Meyer, & Sadowsky, 1984), focuses on the examination of the breast by scanning at a limited angle (Helvie, 2010; Niklason et al., 1997; Wu et al., 2004). For reconstructing three-dimensional (3D) images of the part of the body, the algebraic reconstruction technique (ART) introduced by (Kaczmarz, 1937) and the simultaneous ART (SART) introduced by (Andersen & Kak, 1984) have been used as iterative algorithms, while the filtered back projection (FBP) which was first advanced by Riddle and Bracewell in 1967 (Bracewell & Riddle, 1967) and independently in 1971, by Lakshminarayanan and Ramachandran (Ramachandran & Lakshminarayanan, 1971) has been used as an analytical algorithm, (Kak, Slaney, & Wang, 2002). Whether it is an iterative or analytical method, in

[1] adempolat@comu.edu.tr
*Sorumlu Yazar / Corresponding Author

modalities such as OAT, OT, DOT, CT and DBT, the geometry of the x-rays sent to the target object should be calculated for 3D image reconstruction system design.

The Siddon algorithm (Siddon, 1985), which effectively calculates the ray path geometry, can be used to calculate the system matrix elements in constructing the 3D image reconstruction space. The Siddon algorithm was applied in many applications in ray-path calculation studies and in medical imaging (Gao, 2012; Jacobs et al., 1998; Li et al., 2008; Polat & Yildirim, 2018; Polat et al., 2019a; Xue, Zhang, & Pan, 2011; Zhao & Reader, 2003). There are six main sections in the Siddon algorithm including calculating the range of alpha-parametric values, calculating the range of the indices at x-y-z axes, calculating the alpha-parametric sets for x-y-z axes, merging sets to form alpha-set, calculating voxel intersection length, and calculating voxel indices, respectively.

In the alpha-set creation section of the Siddon algorithm, the alpha-set elements are sorted from small to large, but some elements have the same value or zero-value. The values in the set are used to calculate the voxel intersection length and voxel indices, therefore it is a critical issue to consider whether eliminating some values of zero and/or identical or not. This situation may lead to data loss in the applications of the Siddon algorithm for 3D image reconstructions in medical imaging such as DBT and CT. Considering the mentioned problems, in this study, we analyzed the creation steps of the alpha-parametric set that affect the calculations of voxel intersection length and voxel indices and investigated the effect of using or eliminating the repetitive and/or zero- values for the calculations in the Siddon algorithm.

## 2. Materials and Methods

The Siddon algorithm introduced an efficient, reliable, and exact calculation of a radiological route through a 3D-array of CT (Siddon, 1985). The schematic of two-dimensional (2D) representation for the 3D CT array of ($N_x$, $N_y$, $N_z$) voxels is given in Figure 1. A single ray starting from point $P_1(x_1, y_1)$ to point $P_2(x_2, y_2)$ passes through the CT array. The radiological path in 3D space, in other words, the ray sum is defined by 2.1.

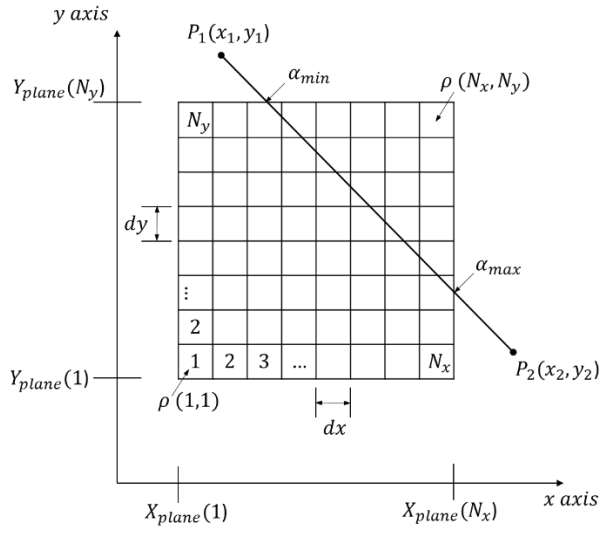


Figure 1. The schematic of two-dimensional (2D) representation for the 3D CT array of ($N_x$, $N_y$, $N_z$) voxels

$$d = \sum_i \sum_j \sum_k l(i,j,k)\rho(i,j,k) \tag{2.1}$$

where $l(i,j,k)$ is the voxel intersection length and $\rho(i,j,k)$ is the density of voxel in the point $(i,j,k)$.

In the Siddon algorithm, the ray from $P_1(x_1, y_1, z_1)$ to $P_2(x_2, y_2, z_2)$ is described with the alpha-parametric set; $\alpha$ ($\alpha_1 = 0$ at $P_1$ and $\alpha_2 = 1$ at $P_2$) in 3D space (see 2.2).

$$X(\alpha) = X_1 + \alpha(X_2 - X_1)$$
$$Y(\alpha) = Y_1 + \alpha(Y_2 - Y_1) \quad (2.2)$$
$$Z(\alpha) = Z_1 + \alpha(Z_2 - Z_1)$$

Alpha-parameter ($\alpha$) set in the range of ($\alpha_{min}, \alpha_{max}$) indicates the intersections of the ray with planes. If $P_1$ or $P_2$ are within the grid boundaries, then $\alpha_{min}$ gets zero, and $\alpha_{max}$ gets one, otherwise they become a nonzero value (see Figure 1).

For the ($N_x$, $N_y$, $N_z$) voxel array, orthogonal sets of equidistant parallel planes are written as in 2.3.

$$X_{plane}(i) = X_{plane}(1) + (i-1)dx \qquad i = 1, 2, \dots, N_x$$
$$Y_{plane}(j) = Y_{plane}(1) + (j-1)dy \qquad j = 1, 2, \dots, N_y \quad (2.3)$$
$$Z_{plane}(k) = Z_{plane}(1) + (k-1)dz \qquad k = 1, 2, \dots, N_z$$

where $dx, dy,$ and $dz$ are the dimensions of the voxel and the distances between the $x, y, z$ planes.

The $\alpha$ -parametric values are calculated by 2.4 using 2.2 and 2.3.

$$if\ X_2 \neq X_1,$$
$$\alpha_x(1) = \left[X_{plane}(1) - X_1\right]/(X_2 - X_1) \quad (2.4)$$
$$\alpha_x(N_x) = \left[X_{plane}(N_x) - X_1\right]/(X_2 - X_1)$$

Expressions are similar for $y$ and $z$ planes for $\alpha_y(1)$, $\alpha_y(N_y)$, $\alpha_z(1)$, and $\alpha_z(N_z)$. After that $\alpha_{min}$ and $\alpha_{max}$ are calculated by 2.5.

$$\alpha_{min} = max\{1, min[\alpha_x(1), \alpha_x(N_x)], min[\alpha_y(1), \alpha_y(N_y)], min[\alpha_z(1), \alpha_z(N_z)]\}$$
$$\alpha_{max} = min\{1, max[\alpha_x(1), \alpha_x(N_x)], max[\alpha_y(1), \alpha_y(N_y)], max[\alpha_z(1), \alpha_z(N_z)]\} \quad (2.5)$$

In the case $\alpha_{min}$ is greater than or equal to $\alpha_{max}$, the voxels are not intersected by the ray. $\alpha_{min}$ and $\alpha_{max}$ values are used to calculate the indices range of ($i_{min}, i_{max}$), ($j_{min}, j_{max}$) and ($k_{min}, k_{max}$), which intersect the planes (2.6).

$$if\ (X_2 - X_1) \geq 0,$$
$$i_{min} = N_x - \left[X_{plane}(N_x) - \alpha_{min}(X_2 - X_1) - X_1\right]/dx$$
$$i_{max} = 1 + \left[X_1 + \alpha_{max}(X_2 - X_1) - X_{plane}(1)\right]/dx$$
$$if\ (X_2 - X_1) \leq 0, \quad (2.6)$$
$$i_{min} = N_x - \left[X_{plane}(N_x) - \alpha_{max}(X_2 - X_1) - X_1\right]/dx$$
$$i_{max} = 1 + \left[X_1 + \alpha_{min}(X_2 - X_1) - X_{plane}(1)\right]/dx$$

The similar notations are written for $j_{min}, j_{max}$, $k_{min}$, and $k_{max}$. Using these indices, the sets of alpha values ($\{\alpha_x\}, \{\alpha_y\}, \{\alpha_z\}$) which represent the intersections of the ray with the $x, y, z$ planes are calculated as in 2.7 for $\{\alpha_x\}$, and with similar expressions for $\{\alpha_y\}$, and $\{\alpha_z\}$.

$$if\ (X_2 - X_1) > 0,$$
$$\{\alpha_x\} = \{\alpha_x(i_{min}), \dots, \alpha_x(i_{max})\} \quad (2.7)$$
$$if\ (X_2 - X_1) < 0,$$
$$\{\alpha_x\} = \{\alpha_x(i_{max}), \dots, \alpha_x(i_{min})\}$$

The definite intersections are determined by merging the sets ($\alpha_{min}, \alpha_{max}$), $\{\alpha_x\}, \{\alpha_y\}$, and $\{\alpha_z\}$ as alpha-parametric set. The merged alpha-parametric set $\{\alpha\}$ that has $n + 1$ elements is expressed as in 2.8.

$$\{\alpha\} = \{\alpha_{min}, merge[\{\alpha_x\},\{\alpha_y\},\{\alpha_z\}], \alpha_{max}\}$$
$$\{\alpha\} = \{\alpha(0), \alpha(1), \dots, \alpha(n)\} \quad (2.8)$$

The difference of two consecutive terms in the alpha set is used to calculate the intersection length $l(m)$ in 2.9. $d_{12}$ in 2.9 is the Euclidian distance (the total length) of the ray from $P_1$ to $P_2$, and the formulation of it is given in 2.10. Once the $\{\alpha\}$ array is formed, the exploring of the voxels that are hit with the ray and the calculations of their intersection lengths are possible. The $mth$ and $(m-1)th$ values of the $\{\alpha\}$ array, which are the parametric weights of the intersected voxels, form the intersection length as in 2.9.

$$l(m) = d_{12}[\alpha(m) - \alpha(m-1)] \quad \text{for } m = 1,2,3,\dots,n \quad (2.9)$$

$$d_{12} = \sqrt{(X_2 - X_1)^2 + (Y_2 - Y_1)^2 + (Z_2 - Z_1)^2} \quad (2.10)$$

The voxel indices $[i(m), j(m), k(m)]$ which intersected by the ray are calculated using the midpoint of two consecutive intersections *($mth$* and $(m-1)th$ alpha*)* as in 2.11.

$$i(m) = 1 + \left[X_1 + \alpha_{mid}(X_2 - X_1) - X_{plane}(1)\right]/dx$$
$$j(m) = 1 + \left[Y_1 + \alpha_{mid}(Y_2 - Y_1) - Y_{plane}(1)\right]/dy \quad (2.11)$$
$$k(m) = 1 + \left[Z_1 + \alpha_{mid}(Z_2 - Z_1) - Z_{plane}(1)\right]/dz$$

where the $\alpha_{mid}$ is the midpoint of the $mth$ and $(m-1)th$ alpha and is given by 2.12.

$$\alpha_{mid} = [\alpha(m) + \alpha(m-1)]/2 \quad (2.12)$$

Finally, the projection value, $P_\theta$, which is the radiological route can be obtained by summing over the $n$ elements of the length array $l(m)$ obtained from $(n+1)$ elements of $\{\alpha\}$-parametric set multiplied by the densities of the voxels as in 2.13.

$$P_\theta = \sum_{m=1}^{n} l(m)\rho[i(m), j(m), k(m)] \quad (2.13)$$

where $\rho[i(m), j(m), k(m)]$ is the $mth$ voxel density and $\theta$ is the projection angle.

The intersection lengths $l(m)$ for each ray are used to build up a system matrix $\boldsymbol{A}$ for all projections (in this study, three projections, $\theta = -25^0, 0^0, +25^0$), and this system matrix $\boldsymbol{A}$ is used to provide a solution for linear algebraic equation system given by 2.14, which models 3D image reconstruction. In 2.14, $P_\theta$ is the projections acquired from a target via a medical imaging modality such as CT and DBT, $v$ is the vector form of the voxels of the target, and $\boldsymbol{A}$ is the system matrix calculated by the Siddon algorithm.

$$P_\theta = \boldsymbol{A}.v \quad (2.14)$$

To build up a system matrix ($\boldsymbol{A}$) using the Siddon algorithm, we created a 2×2×2-size voxel cube model (8 voxels) by assigning $N_x = 2,\ N_y = 2,$ and $N_z = 2$ to analyze the calculated alpha-parametric set. Then we set a central ray starting point from $P_1(0,0,7)$ to $P_2(0,0,-2)$ to scan 2×2×2-size voxel cube. We also rotated the ray with $-25^0$and $+25^0$ around the rotating point $(0,0,0)$ which is the center of the cube model, thus obtained three projections for data acquisitions of the cube. The visualization of 3-projected system is given in Figure 2.

We calculated and sorted in ascending order the alpha-parametric set for the 2×2×2 model applying the Siddon algorithm. However due to the creation of the same values after performing 2.8, in the length calculation (2.9), the term $\alpha(m) - \alpha(m-1)$ produced 0 that also cause the 0 value of $l(m)$. To get rid of zero-value intersection length problem which causes data loss in the system matrix of 3D image reconstruction modality

as defined in 2.14, we applied a function after performing 2.8, for ensuring two consecutive elements in the alpha-parametric set were not having of the same value. The unique function in Matlab 2018b (license number: 40731897) was applied to the alpha set for eliminating the same values in order not to cause data loss. The flowchart of the proposed method is demonstrated in Figure 3.

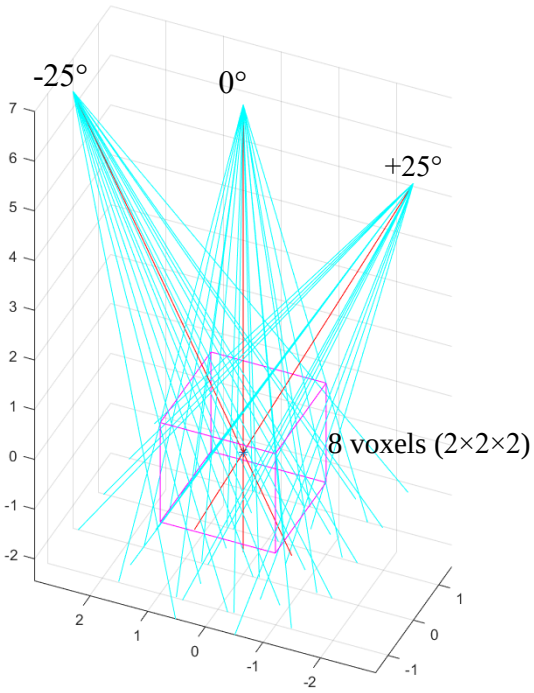


Figure 2. The visualization of the projection acquisition at θ=-25°, 0°, +25° for 2×2×2-size (8 voxels) model of the Siddon algorithm

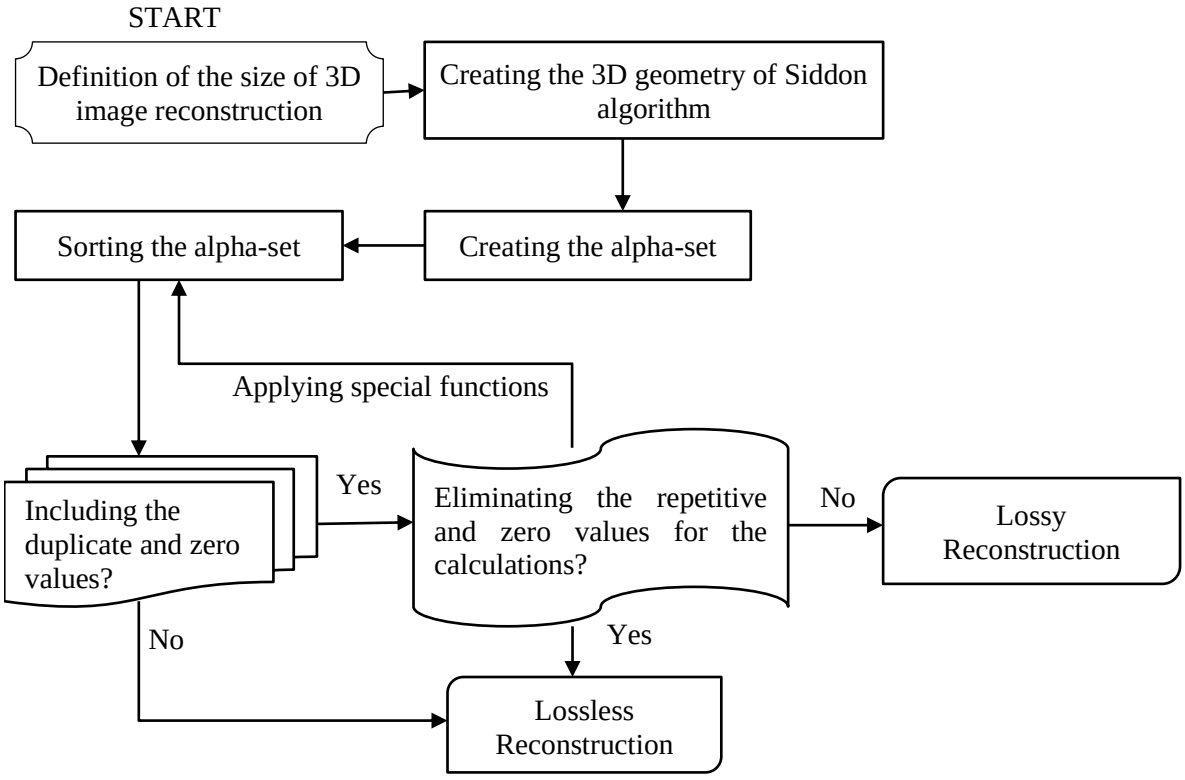


Figure 3. The flowchart of the proposed method

For a further and detailed analysis of data loss within the scope of the investigation of the alpha-parametric set, we 3D-reconstructed the images (with the size of 100×100×50) of a synthetic multilayer phantom (8 mm × 8 mm × 500 μm) mimicking different microchannel (with ~200 μm width and thickness) media separated with the various geometric structures (a circle, a square, and a diamond). For 3D image reconstruction, the 11 projection images (2D: 100×100) of the synthetic phantom obtained from the mini-Opto tomography platform (Polat et al., 2019b) in the range of +/-25° were used. The representation of the reference projection (100×100) of the phantom both in the mini-Opto tomography platform imager and in Matlab 2018b is given in Figure 4.

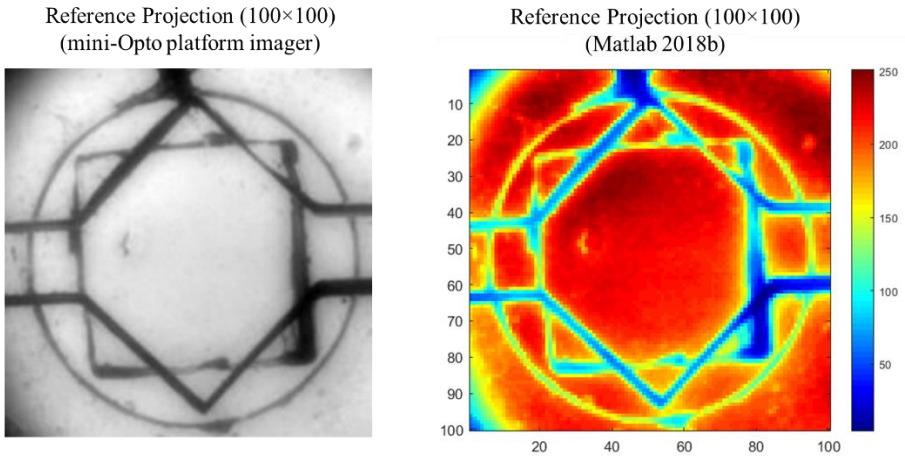


Figure 4. The representation of the reference projection (100×100) of the synthetic multilayer phantom mimicking different microchannel media separated with various geometric structures as a circle, a square, and a diamond both in the mini-Opto tomography platform imager (left) and in Matlab 2018b (right)

## 3. Results and Discussion

According to the acquisition geometry (2×2×2) described in the section of Materials and Methods, alpha-parametric set was calculated using (2.8) for the projections of -25°, 0°, and +25°, and is given in the column of sorted alpha values without the unique function (column-2) in Table 1. It is clear that the repetitive values (0.6667, 0.8889, 2.0 for 6th ray, 0.6667, 0.8889 for 7th and 10th rays, 0.0, 0.6667, 0.8889 for 11th ray) that cause data loss in the system matrix were created in the set (system matrix without the unique function column in Table 2). The values of voxels of 1, 2, 3, and 4 at rays 6, 7, 10, and 11, respectively, shown in the column of system matrix without the unique function (8 voxels) were 0.0, which means data lost. Moreover, this situation may lead to huge data loss in 3D image reconstructions in medical imaging especially for huge dimensions such as size up to 800×800×50. However, using the unique function, we eliminated the same values from the set so that the system matrix conserves the data, which is used in 3D image reconstruction. Additionally, using (2.5) the range alpha-set is limited between the values of min-alpha (0.6667) and max-alpha (0.8889), thus the values of 0.0 and 2.0 were also eliminated from final alpha set which is given in the last column, sorted alpha values with the unique function, of Table 1. Thanks to this result, the values (1.003) of voxels of 1, 2, 3, and 4 at rays 6, 7, 10, and 11, respectively, shown in the column of system matrix with the unique function (8 voxels) in Table 2, were created and data loss was prevented.

Table 1
Sorted alpha-set with and without the unique function at the projections of -25°, 0°, and +25°

| Ray values | Sorted alpha values without the unique function | Min-alpha | Max-alpha | Sorted alpha values with the unique function |
|---|---|---|---|---|
| 6 | 0.6667, 0.6667, 0.7778, 0.8889, 0.8889, 2.0, 2.0 | 0.6667 | 0.8889 | 0.6667, 0.7778, 0.8889 |
| 7 | 0.0, 0.6667, 0.6667, 0.7778, 0.8889, 0.8889, 2.0 | 0.6667 | 0.8889 | 0.6667, 0.7778, 0.8889 |
| 10 | 0.0, 0.6667, 0.6667, 0.7778, 0.8889, 0.8889, 2.0 | 0.6667 | 0.8889 | 0.6667, 0.7778, 0.8889 |
| 11 | 0.0, 0.0, 0.6667, 0.6667, 0.7778, 0.8889, 0.8889 | 0.6667 | 0.8889 | 0.6667, 0.7778, 0.8889 |

Table 2
System matrix with and without the unique function at the projections of -25°, 0°, and +25°

| Ray | System matrix without the unique function (8 voxels) | | | | | | | |
|---|---|---|---|---|---|---|---|---|
| 1 | 0.0 | 0.0 | 0.0 | 0.0 | 0.0 | 0.0 | 0.0 | 0.0 |
| 2 | 0.0 | 0.0 | 0.0 | 0.0 | 0.0 | 0.0 | 0.0 | 0.0 |
| 3 | 0.0 | 0.0 | 0.0 | 0.0 | 0.0 | 0.0 | 0.0 | 0.0 |
| 4 | 0.0 | 0.0 | 0.0 | 0.0 | 0.0 | 0.0 | 0.0 | 0.0 |
| 5 | 0.0 | 0.0 | 0.0 | 0.0 | 0.0 | 0.0 | 0.0 | 0.0 |
| 6 | 0.0 | 0.0 | 0.0 | 0.0 | **1.003** | 0.0 | 0.0 | 0.0 |
| 7 | 0.0 | 0.0 | 0.0 | 0.0 | 0.0 | 0.0 | **1.003** | 0.0 |
| 8 | 0.0 | 0.0 | 0.0 | 0.0 | 0.0 | 0.0 | 0.0 | 0.0 |
| 9 | 0.0 | 0.0 | 0.0 | 0.0 | 0.0 | 0.0 | 0.0 | 0.0 |
| 10 | 0.0 | 0.0 | 0.0 | 0.0 | 0.0 | **1.003** | 0.0 | 0.0 |
| 11 | 0.0 | 0.0 | 0.0 | 0.0 | 0.0 | **0.0** | 0.0 | **1.003** |
| Ray | System matrix with the unique function (8 voxels) | | | | | | | |
| 1 | 0.0 | 0.0 | 0.0 | 0.0 | 0.0 | 0.0 | 0.0 | 0.0 |
| 2 | 0.0 | 0.0 | 0.0 | 0.0 | 0.0 | 0.0 | 0.0 | 0.0 |
| 3 | 0.0 | 0.0 | 0.0 | 0.0 | 0.0 | 0.0 | 0.0 | 0.0 |
| 4 | 0.0 | 0.0 | 0.0 | 0.0 | 0.0 | 0.0 | 0.0 | 0.0 |
| 5 | 0.0 | 0.0 | 0.0 | 0.0 | 0.0 | 0.0 | 0.0 | 0.0 |
| 6 | **1.003** | 0.0 | 0.0 | 0.0 | **1.003** | 0.0 | 0.0 | 0.0 |
| 7 | 0.0 | 0.0 | **1.003** | 0.0 | 0.0 | 0.0 | **1.003** | 0.0 |
| 8 | 0.0 | 0.0 | 0.0 | 0.0 | 0.0 | 0.0 | 0.0 | 0.0 |
| 9 | 0.0 | 0.0 | 0.0 | 0.0 | 0.0 | 0.0 | 0.0 | 0.0 |
| 10 | 0.0 | **1.003** | 0.0 | 0.0 | 0.0 | **1.003** | 0.0 | 0.0 |
| 11 | 0.0 | 0.0 | 0.0 | **1.003** | 0.0 | 0.0 | 0.0 | **1.003** |

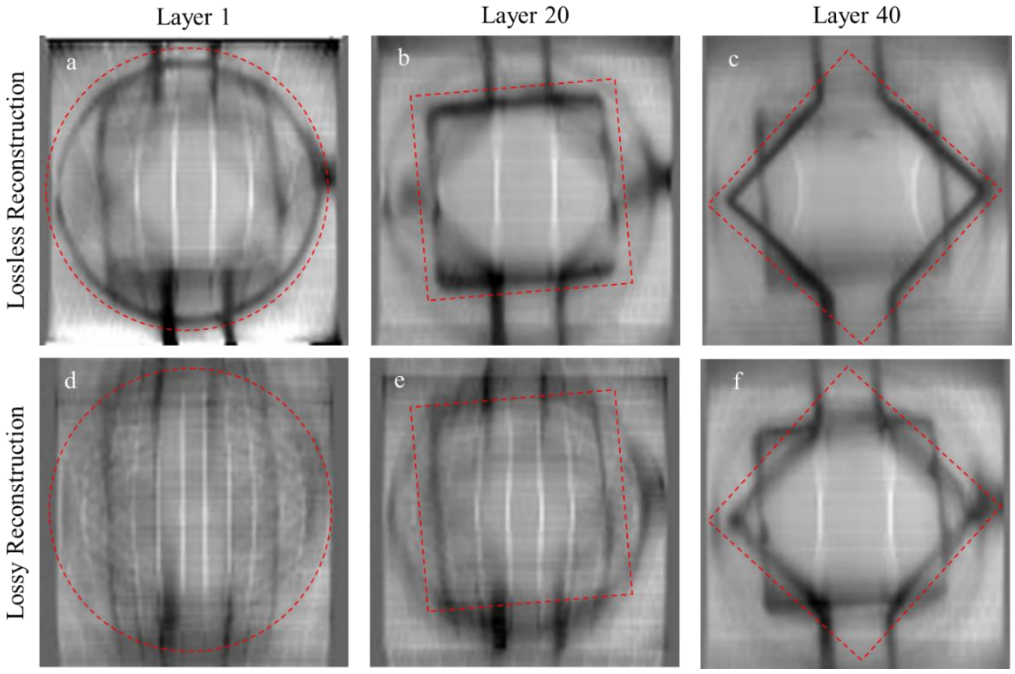


Figure 5. Lossless (first row: a, b, and c) and lossy (second row: d, e, and f) reconstruction. The geometric structures of the circle (a), the square (b), and the diamond (c) were captured in the layers of 1 (a), 20 (b), and 40 (c), respectively applying system matrix with the unique function (lossless reconstruction). The geometric structures of the circle (d), the square (e), and the diamond (f) could not captured in the layers of 1 (d), 20 (e), and 40 (f), respectively applying system matrix without the unique function (lossy reconstruction)

In this study, we tested and validated the effects of alpha-set on reconstructed images of the synthetic multilayer phantom that includes the geometric structures of the circle, the square, and the diamond with the size of 100×100×50 (Figure 5). When Figure 5 is examined, the first row (a, b, and c) are the lossless reconstruction, which means the system matrix was implemented with the unique function. However, the second row (d, e, and f) are the lossy reconstruction, which means the system matrix was implemented without the unique function. In the qualitative assessment, it is clear that the circle, the square, and the diamond shapes in the lossless reconstruction were captured in the layers of 1, 20, and 40, respectively. Applying special functions in Matlab 2018b (e.i. unique function), the repetitive and zero-values of the alpha-parametric set were eliminated for the ray path calculations and lossless reconstruction. Therefore, the importance and the effect of alpha-set analysis in Siddon algorithm on reconstructed images should be taken into consideration in medical imaging modalities to avoid lossy reconstruction.

Evaluating the calculation values of alpha set and system matrix, we strongly recommend using the unique function after (2.8) step in the Siddon algorithm to avoid loss in data in system matrix for the 3D image reconstruction modality.

## 4. Conclusion

The Siddon algorithm provides an efficient radiological path calculation for building up the system matrix which is used in 3D image reconstruction applications such as computed tomography (CT) and digital breast tomosynthesis (DBT) modalities. The system matrix includes the voxel array and intersection length array for the interaction of the ray with the target object and is used to reconstruct the projections acquired from the target for 3D imaging. Thus, obtaining correct data in the system matrix by the Siddon algorithm is a very critical issue. The value of the elements of the system matrix is calculated by performing the calculation step of alpha-set parameters in the Siddon algorithm. Due to appearing the consecutive values of some elements, the intersection length calculation produces zero values that cause data loss in 3D image reconstruction. In this study, we proposed an additional step in order to eliminate the same values of the consecutive values of the alpha-parameter set which cause zero-valued intersection lengths. We performed both the Siddon algorithm in the regular process and the Siddon algorithm with the additional step we proposed to avoid zero-valued of the intersection length. Comparing the results in the system matrix for both methods, our proposal for the Siddon algorithm provided not produce zero-valued of intersection length, thus avoiding the data loss in the system matrix which is used in 3D image reconstructions in medical imaging. We proved our proposal by validating the concept with the lossy and lossless 3D image reconstruction of a 100×100×50 size-synthetic phantom. For future work, we aim to perform and test our proposal for the Siddon algorithm for the increased dimensions of the system and applying it to the realistic phantoms

## Acknowledgement

This work was supported by TUBITAK, the Scientific and Research Council of Turkey, under the project number 119E388.

## Author Contributions

Adem Polat: Conceived the original concept, designed the analysis and wrote the manuscript.

## Conflicts of Interest

The authors declare no conflict of interest.

**References**

Andersen, A. H., & Kak, A. C. (1984). Simultaneous Algebraic Reconstruction Technique (SART): A Superior Implementation of the Art Algorithm. *Ultrason. Imag. 6*(1), 81–94. DOI: https://doi.org/10.1016/0161-7346(84)90008-7

Biguri, A., Dosanjh, M., Hancock, S., & Soleimani, M. (2017). A general method for motion compensation in x-ray computed tomography. *Physics in Medicine & Biology*, 62(16), 6532. Retrieved from: https://iopscience.iop.org/article/10.1088/1361-6560/aa7675/meta

Bracewell, R. N., & Riddle, A. C. (1967). Inversion of Fan-Beam Scans in Radio Astronomy. *The Astrophysic. Journ.* 150:427. Retrieved from: http://adsabs.harvard.edu/full/1967ApJ...150..427B

Dekker, K. H., Battista, J. J., & Jordan, K. J. (2017). Evaluation of an iterative reconstruction algorithm for optical CT radiation dosimetry. *Medical physics*, 44(12), 6678-6689. DOI: https://doi.org/10.1002/mp.12635

Gao, Hao. (2012). Fast Parallel Algorithms for the X-Ray Transform and Its Adjoint. *Medical Physics 39*(11), 7110–20. DOI: https://doi.org/10.1118/1.4761867

Helvie, M. A. (2010). Digital Mammography Imaging: Breast Tomosynthesis and Advanced Applications. *Radiolog. Clin. of North America 48*(5), 917–29. DOI: https://dx.doi.org/10.1016%2Fj.rcl.2010.06.009

Jacobs, F., Sundermann, E., Sutter, B. D., Christiaens, M., & Lemahieu, I. (1998). A Fast Algorithm to Calculate the Exact Radiological Path through a Pixel or Voxel Space. *J. of Computing and Information Technology 6*(1), 89–94. Retrieved from: https://hrcak.srce.hr/index.php?show=clanak&id_clanak_jezik=221195&lang=en

Kaczmarz, S. (1937). Angenäherte Auflösung von Systemen Linearer Gleichungen (English Translation by Jason Stockmann: Approximate Solution of Systems of Linear Equations). *Bulletin International de l'Académie Polonaise Des Sciences et Des Lettres*. *35*, 355–357. Retrieved from: https://ntrl.ntis.gov/NTRL/dashboard/searchResults/titleDetail/UCRLTRANS10985.xhtml

Kak, A. C., Slaney, M., & Wang, G. (2002). Principles of Computerized Tomographic Imaging. *Medical Physics 29*(1), 107–107. DOI: https://doi.org/10.1118/1.1455742

Klose, A. D., & Hielscher, A. H. (1999). Iterative reconstruction scheme for optical tomography based on the equation of radiative transfer. *Medical Physics*, 26(8), 1698-1707. DOI: https://doi.org/10.1118/1.598661

Kopans, D. B., Meyer, J. E., & Sadowsky, N. (1984). Breast Imaging. *New England Journal of Medicine 310*(15), 960–67. DOI: 10.1056/NEJM198404123101506. Retrieved from: https://www.nejm.org/doi/pdf/10.1056/NEJM198404123101506

Li, N., Zhao, H. X., Cho, S. H., Choi, J. G. & Kim, M. H. (2008). A Fast Algorithm for Voxel-Based Deterministic Simulation of X-Ray Imaging. *Computer Physics Communications 178*(7), 518–23. DOI: https://doi.org/10.1016/j.cpc.2007.11.008

Mercan, T., Sevim, G., Kazancı, H. Ö., Üncü, Y. A., & Canpolat, M. (2017). Comparison of Images Produced by Diffuse Optical Tomography with Two Different Backscatter Techniques. *In 2017 21st National Biomedical Engineering Meeting (BIYOMUT)* (pp. i-iv). IEEE. Retrieved from: https://ieeexplore.ieee.org/abstract/document/8479038

Mercan, T., Sevim, G., Üncü, Y. A., Serkan, U. S. L. U., Kazancı, H. Ö., & Canpolat, M. (2019). The Comparison of Reconstruction Algorithms for Diffuse Optical Tomography. *Süleyman Demirel Üniversitesi Fen Edebiyat Fakültesi Fen Dergisi*, 14(2), 285-295. Retrieved from: https://dergipark.org.tr/en/pub/sdufeffd/issue/50336/549528

Niklason, L. T., Christian, B. T., Niklason, L. E., Kopans, D. B., Castleberry, D. E., Opsahl-Ong, B. H., .... & Wirth, R. F. (1997). Digital Tomosynthesis in Breast Imaging. *Radiology 205*(2), 399–406. Retrieved from: https://pubs.rsna.org/doi/pdf/10.1148/radiology.205.2.9356620

Nobel Media AB. 2014. "The Official Website of the Nobel Prize - NobelPrize.Org." *Godfrey N. Hounsfield – Biographical. Nobel Media AB.* Retrieved from: https://www.nobelprize.org/

Oliveira, N., Mota, A. M., Matela, N., Janeiro, L., & Almeida, P. (2016). Dynamic relaxation in algebraic reconstruction technique (ART) for breast tomosynthesis imaging. Computer methods and programs in

biomedicine, 132, 189-196. Retrieved from: https://www.sciencedirect.com/science/article/pii/S0169260715301590

Paltauf, G., Viator, J. A., Prahl, S. A., & Jacques, S. L. (2002). Iterative reconstruction algorithm for optoacoustic imaging. *The Journal of the Acoustical Society of America*, 112(4), 1536-1544. DOI: https://doi.org/10.1121/1.1501898

Polat, A., & Yildirim, I. (2018). An Iterative Reconstruction Algorithm for Digital Breast Tomosynthesis Imaging Using Real Data at Three Radiation Doses. *Journal of X-Ray Science and Technology 26*(3), 347–60. DOI: 10.3233/XST-17320. Retrieved from: https://content.iospress.com/articles/journal-of-x-ray-science-and-technology/xst17320

Polat, A., Matela N., Dinler, A., Zhang, Y. S. & Yildirim, I. (2019a). Digital Breast Tomosynthesis Imaging Using Compressed Sensing Based Reconstruction for 10 Radiation Doses Real Data. *Biomedical Signal Processing and Control 48*, 26–34. DOI: https://doi.org/10.1016/j.bspc.2018.08.036

Polat, A., Hassan, S., Yildirim, I., Oliver, L. E., Mostafaei, M., Kumar, S., ... & Zhang, Y. S. (2019b). A miniaturized optical tomography platform for volumetric imaging of engineered living systems. *Lab on a Chip*, 19(4), 550-561. DOI: 10.1039/C8LC01190G. Retrieved from: https://pubs.rsc.org/no/content/articlehtml/2019/lc/c8lc01190g

Raju, T. N. (1999). The Nobel Chronicles. 1979: Allan MacLeod Cormack (b 1924); and Sir Godfrey Newbold Hounsfield (b 1919). *Lancet 354*(9190), 1653. DOI: https://doi.org/10.1016/S0140-6736(05)77147-6

Ramachandran, G. N., & Lakshminarayanan, A. V. (1971). Three-Dimensional Reconstruction from Radiographs and Electron Micrographs: Application of Convolutions Instead of Fourier Transforms. *Proc. Nat. Acad. Sci. 68*(9), 2236-2240. DOI: https://doi.org/10.1073/pnas.68.9.2236

Sevim, G., Merçan, T., Üncü, Y. A., & Canpolat, M. (2017). A new reconstruction technique used in Diffuse Optical Tomography System. *In 2017 21st National Biomedical Engineering Meeting (BIYOMUT)* (pp. i-iv). IEEE. Retrieved from: https://ieeexplore.ieee.org/abstract/document/8478965

Siddon, R. L. (1985). Fast Calculation of the Exact Radiological Path for a Three-dimensional CT Array. *Medical Physics 12*(2), 252–55. DOI: https://doi.org/10.1118/1.595715

Sidky, E. Y., Kao, C. M., & Pan, X. (2006). Accurate image reconstruction from few-views and limited-angle data in divergent-beam CT. *Journal of X-ray Science and Technology*, 14(2), 119-139. Retrieved from: https://content.iospress.com/articles/journal-of-x-ray-science-and-technology/xst00155

Üncü, Y. A., Merçan, T., Canpolat, M., & Sevim, G. (2017). A new approach to image processing in diffuse optical tomography and 3-D image. *In 2017 25th Signal Processing and Communications Applications Conference (SIU)* (pp. 1-4). IEEE. Retrieved from: https://ieeexplore.ieee.org/abstract/document/7960192

Wang, K., Su, R., Oraevsky, A. A., & Anastasio, M. A. (2012). Investigation of iterative image reconstruction in three-dimensional optoacoustic tomography. *Physics in Medicine & Biology*, 57(17), 5399. Retrieved from: https://iopscience.iop.org/article/10.1088/0031-9155/57/17/5399/pdf

Wu, T., Moore, R. H., Rafferty, E. A., & Kopans, D. B. (2004). A Comparison of Reconstruction Algorithms for Breast Tomosynthesis. *Medical Physics 31*(9), 2636–47. DOI: https://doi.org/10.1118/1.1786692

Xue, Z., Zhang, L., & Pan, J. (2011). A New Algorithm for Calculating the Radiological Path in CT Image Reconstruction. *Proceedings of 2011 Internation. Confer. on Electronic and Mechanical Eng. and Information Technology* (pp. 4527–30). Harbin. DOI: 10.1109/EMEIT.2011.6024036. Retrieved from: https://ieeexplore.ieee.org/abstract/document/6024036

Zhao, H., & Reader, A.J. (2003). Fast Ray-Tracing Technique to Calculate Line Integral Paths in Voxel Arrays. *IEEE Nuclear Science Symposium Conference Record (IEEE Cat. No.03CH37515)*. (pp. 2808–12). Portland, OR, USA. DOI: 10.1109/NSSMIC.2003.1352469. Retrieved from: https://ieeexplore.ieee.org/abstract/document/1352469